Holography of particle tracks in the Fermilab 15-Foot Bubble Chamber

E-632 Collaboration *

H. Bingham and J. Lys
University of California, Berkeley, CA 94720, USA

L. Verluyten [1,10] and S. Willocq [2]
Interuniversity Institute for High Energies (ULB-VUB), B-1050 Brussels, Belgium, and Fermilab, Batavia, IL 60510, USA

J. Moreels
Interuniversity Institute for High Energies (ULB-VUB), B-1050 Brussels, Belgium

K. Geissler, G.G. Harigel and D.R.O. Morrison
CERN, CH-1211 Geneva 23, Switzerland

F. Bellinger [3], H. Bjelkhagen [4], H. Carter, J. Ellermeier, J. Foglesong, J. Hawkins, J. Kilmer, T. Kovarik, W. Smart, J. Urbin, L. Voyvodic, E. Wesly [5] and W. Williams
Fermilab, Batavia, IL 60510, USA

R.J. Cence and M.W. Peters
University of Hawaii, Honolulu, HI 96822, USA

R.A. Burnstein and R. Naon
Illinois Institute of Technology, Chicago, IL 60616, USA

P. Nailor [6]
Imperial College, London SW7, UK

M. Aderholz
Max-Planck-Institut für Physik und Astrophysik, D-8000 München 40, FRG

G. Corrigan [7]
University of Oxford, Oxford OX1 3RH, UK

R. Plano

Rutgers University, New Brunswick, NJ 08903, USA

R.L. Sekulin and S. Sewell [8]

Rutherford Appleton Laboratories, Didcot OX110QX, UK

E.B. Brucker

Stevens Institute of Technology, Hoboken, NJ 07030, USA

H. Akbari [9], R.H. Milburn, D. Passmore and J. Schneps

Tufts University, Medford, MA 02155, USA

Received 9 February 1990 and in revised form 5 July 1990

During a quadrupole–triplet neutrino experiment with the 15-Foot Bubble Chamber at Fermilab, a large number of events was recorded on ~110000 good holograms, which were taken simultaneously with the conventional three-view photographs. The holograms allow the study of event vertices in a large volume with greatly improved resolution. The experimental setup and the operation of the system is described. Preliminary results obtained during the replay of holograms with the newly developed real- and virtual-image machines are discussed.

1. Introduction

Holography offers the possibility of photographing large volumes with better resolution than obtainable with conventional optics. This is of particular interest for the study of elementary particle interactions in gaseous or liquid detectors, where one searches for rare interactions with short lifetimes (i.e. short track lengths). The feasibility of this technique had been demonstrated for the first time in a 120-cm^3 bubble chamber (Berne Infinitesimal Bubble Chamber BIBC [1]). The exposure of a 2 l chamber (Holographic Bubble Chamber HOBC [2]) in a hadron beam at CERN resulted in 40000 holograms, which were analyzed. However, bubble chambers operated in neutrino beams are the most useful applications of this technique [3,4]. In the large cryogenic bubble chambers [3] the aim is to holograph bubbles in a volume of up to several cubic meters ~1 ms after their creation, when they have grown to only ~100 μm in diameter. These holograms supplement the conventional stereophotographs of particle tracks taken some ten milliseconds later, when the bubbles have grown to diameters of ~400 μm. These two techniques combine the advantages of a quick overall view, easy event recognition and track measurement in the conven-

tional photographs, with the more detailed picture of the interesting event vertex region in the holograms.

The present paper describes the experience with holography in the 15-Foot Bubble Chamber at Fermilab, gained during a technical run (1984) and two physics runs (1985 and 1987/88). The Chamber was exposed to a quadrupole-triplet neutrino beam with 800 GeV/c protons from the Tevatron on the production target. In the second physics run, 293060 conventional 3-view pictures and ~218000 holograms, of which ~110000 are useful for physics analysis, were recorded simultaneously. The analysis of these photographs and holograms is in progress and some preliminary results from the scanning of the holograms will be presented.

We limit ourselves here to a description of the modified single-beam holography. The basic idea had been developed by C. Baltay of Columbia University [3,5] and was tested earlier in the Big European Bubble Chamber (BEBC) at CERN [6,7]. First results from its application in the 15-Foot Bubble Chamber can be found in refs. [8–11]. The main emphasis of this paper is on the technical aspects of the layout used in the second physics run and on the practical experience with this system. Descriptions of replay machines built for the analysis of these holograms are given in refs. [12–15]. Features of two-beam illumination systems for large volume holography can be found in ref. [16].

In section 2, we describe the theory and design considerations of our modified single-beam technique, with emphasis on the layout of the illumination system, its adaption to the existing geometry of the 15-Foot Bubble Chamber, and on a variety of effects due to

---

[8] Now with Autofile Ltd., Slough, UK.
[9] Now at Johns Hopkins University, Baltimore, MD 21218, USA.
[10] Researcher IIKW, Brussels, Belgium.

nonstatic conditions during the recording of holograms. In section 3, the layout of the holographic system is presented, which includes our modifications of the commercial holographic laser, the transport and monitoring of the laser beam, and the design of the dispersing lens. The synchronisation of the laser pulse with the neutrino beam pulse is briefly described. In section 4 follows an overview of our experience with the system during several months of running. Furthermore, preliminary results obtained during the replay of a small sample of holograms are given, which show that we achieved the expected resolution over a large volume. Section 5 contains a summary of our new developments and a brief outlook on further applications of the technique.

2. Theory and design considerations of the modified single-beam technique

A hologram is formed by the interference of coherent light from a reference beam with the coherent light scattered by objects. In our case the objects are vapour bubbles with a refractive index of ~ 1.0 in a liquid with an index of ~ 1.088.

In two small bubble chambers, operated with liquids above room temperature [1,2], an in-line, or Gabor-type, illumination was used: an expanded parallel laser beam passes through the liquid onto the holographic film. Only a small part of this beam is diffracted by the bubbles and interference between the diffused and non-diffused waves produces fringes which are recorded by the emulsion. For HOBC [2], two-beam geometries were tested, where the reference beam did not pass through the medium to be holographed. Due to the layout of our existing 15-Foot Bubble Chamber, having a volume

more than three orders of magnitude larger than that of the small chamber HOBC, we had to modify the standard holographic techniques.

We describe the experimental scheme (as used in the second physics run), in which the object and reference beam are combined in a new way. The laser beam enters the Bubble Chamber (fig. 1), filled with a 63/37 mol% Ne/H_2 mixture, at its bottom through a specially designed aspheric diverging lens, which also serves as an entrance window. This lens – a sophisticated beam splitter – is designed so that only a small part of the laser light goes through the liquid to a set of three concentric hemispherical windows (fish-eye lenses) on the opposite side of the Chamber directly onto the film. This reference beam exposes completely the 70 mm holographic film format. The rest of the beam illuminates the tracks within a conical volume. The intensity of this object beam is designed to increase at large angles to partly compensate for the decrease of the light scattered by the bubbles at these angles. Some elementary formulas, together with estimates based on experience in the smaller bubble chambers, are given in ref. [6]. The latter contains data on the optical resolution of such a system, the energy needed to illuminate a given volume, the ratio of intensities of object to reference beam, and the required resolution of the photographic emulsion. These data will be re-evaluated in the context of our recent experience. A large coherence length, and a Gaussian-like spatial distribution (TEM$_{00}$ mode) of the beam from the oscillator stage, together with a fairly uniform profile of the amplified laser beam over the aperture of the dispersing lens are important laser beam properties for our experiment.

In applying this modified single-beam technique to holography of tiny bubbles in a cryogenic multi-cubic-
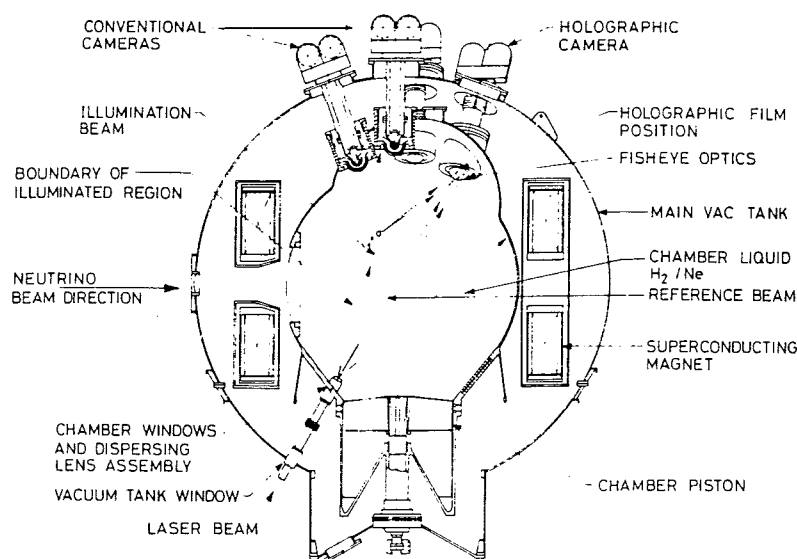

Fig. 1. 15-Foot Bubble Chamber, side view.

meter Bubble Chamber, several disturbing experimental effects had to be controlled. The most serious of these disturbances arise from:

a) excessive heating of the cryogenic liquid by the intense laser light, causing parasitic bubble creation and thereby unwanted scattered light;

b) vibration of the equipment during the mechanical expansion of the liquid; and

c) movement and growth of track bubbles during the laser illumination. Furthermore,

d) multiple scattering of the laser light from the Chamber wall, which is covered with a reflecting material (Scotchlite), can spoil the quality of the hologram, lower the contrast, and decrease the visible volume.

We give here some of the design considerations which govern the choices of laser energy, pulse length, and light distribution inside the Bubble Chamber needed to maximize the volume recorded in the hologram. These considerations also indicate hardware changes which help to achieve this goal.

2.1. Effect of background light (noise) hitting the holographic film

The information available to be recorded on the holographic film is the fringe pattern formed by the interference of the reference beam and the object beam (i.e. the light scattered by a bubble). Therefore, bubbles which give the same fringe modulation M and are at the same Θ_h (fig. 2), will be equally well recorded on the film and be equally bright in the replayed hologram.

We define the Beam Branching Ratio (BBR) as the intensity, on the holographic film, of the laser light scattered from a single bubble, divided by the reference beam intensity. The BBR in this application is given by the formula

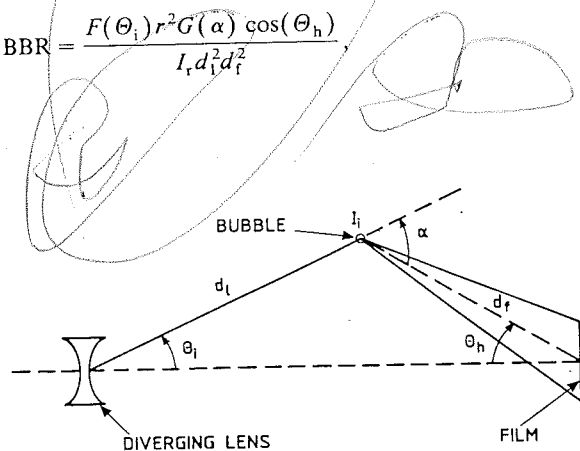$$BBR = \frac{F(\Theta_i) r^2 G(\alpha) \cos(\Theta_h)}{I_r d_1^2 d_f^2},$$

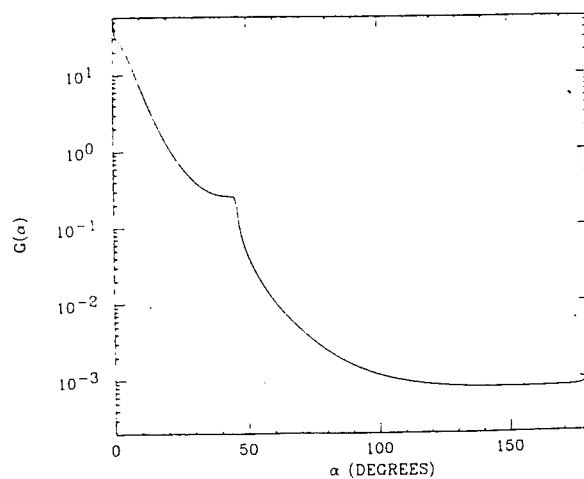Fig. 2. Simplified representation of the holographic setup with the holographic parameters.

Fig. 3. Geometric scattering function $G(\alpha)$ as function of the scattering angle α.

with (fig. 2)

r = bubble radius,

d_1 = distance between the bubble and the dispersing lens,

d_f = distance between the bubble and the holographic film,

Θ_i = illumination angle,

α = scattering angle,

Θ_h = angle between the reference beam and the scattered beam from the bubble at the film,

I_r = reference beam intensity,

$F(\Theta_i)$ = illumination intensity distribution per solid angle,

$G(\alpha)$ = scattering function (fig. 3 [17]).

In the geometry described above, once the light output distribution from the dispersing lens is fixed by the shape of the lens and the spatial distribution of the input laser beam, the BBR is determined (for 100 μm bubbles) at every point in the illuminated volume of the Chamber, and this ratio can be taken over any area on the film. The output energy of the laser is then adjusted to give the proper exposure of the film. We define

I_r = E_r^2 = intensity on the film plane of the reference beam (from the dispersing lens),

I_b = E_b^2 = intensity on the film plane of the light scattered from a bubble,

$BBR = I_b/I_r$,

r = $(BBR)^{1/2} = |E_b|/|E_r|$,

I_x = maximum intensity on film plane (where E_r and E_b constructively interfere),

I_m = minimum intensity on film plane (where E_r and E_b destructively interfere),

M = $(I_x - I_m)/(I_x + I_m)$ = fringe modulation on film plane.

Assuming that $E_r \gg E_b$, then

$$I_x = (E_r + E_b)^2 = E_r^2 + 2E_rE_b,$$

$$I_m = (E_r - E_b)^2 = E_r^2 - 2E_rE_b,$$

$$M = 4E_rE_b/2E_r^2 = 2r.$$

If there are other sources of light hitting the film, this calculation must be modified. In our setup, background laser light (noise from, for example, multiple reflections off the Chamber walls) hitting the film will be proportional to the overall laser intensity and hence proportional to the reference beam intensity, $I_n = kI_r$. The intensity of the light on the film is now

$$I_r + I_n = I_r(1 + k),$$

and we must reduce the overall laser beam intensity to avoid overexposing the film. A new laser intensity of $1/(1 + k)$ times the original will give the same exposure on film:

$$I_{n'} = I_n/(1 + k),$$

$$I_{r'} = I_r/(1 + k),$$

then

$$I_{r'} + I_{n'} = (I_r + I_n)/(1 + k) = (1 + k)I_r/(1 + k) = I_r.$$

Proceeding as above, but including the noise intensity and using

$$I_{x'} = (E_{r'} + E_{b'})^2 + I_{n'},$$

etc. results in

$$M' = 2r/(1 + k),$$

and we see that the net effect of the noise is to reduce the fringe modulation. If the noise were equal to the reference beam ($k = 1$), the laser output must be lowered to one half the original energy and the fringe modulation has been reduced to one half the original value.

Defining BBR$'$ ($= r'^2$) as the Beam Branching Ratio needed, with noise, to get the same fringe modulation as was obtained without noise:

$$M' = M,$$

$$2r'/(1 + k) = 2r,$$

$$r' = r(1 + k), \quad \text{or}$$

$$\text{BBR}' = \text{BBR}(1 + k)^2,$$

thus, the presence of noise requires a higher BBR to obtain the same fringe modulation. In case of noise equal to reference beam intensity, a four times higher BBR is needed.

We then assume that all bubbles whose fringe modulation M is higher than a certain limiting value will be visible in the replayed hologram. The dispersing lens shape was optimized to give the largest volume with a BBR of 0.33×10^{-7} or greater for the lowest light input. Assuming that this corresponds to the M for which a

bubble is just visible, adding noise light equal to the reference beam ($k = 1$) would then require at least a BBR of 1.33×10^{-7} for a bubble to be visible. Referring to fig. 4, one sees that such noise would drastically reduce the volume visible in the hologram.

One source of such noise could be multiple reflections of the laser light inside the Bubble Chamber. The magnitude of this effect can be estimated with a simple calculation: if 10 J of laser light is sent into the Bubble Chamber, the average light intensity on the Chamber walls is 20 μJ/cm^2. The holographic film is part of the wall and requires ~ 0.9 μJ/cm^2-laser light to give the desired density. The average noise light is ~ 20 times the intended point source reference beam, indicating a potential problem. During the first physics run, hologram quality was degraded if more than ~ 0.6 J of laser light was sent into the Bubble Chamber. To solve this problem, baffles were designed and installed on the Chamber walls for the second physics run. These baffles trapped and absorbed the laser light after it had crossed the Chamber once (section 4.1).

Another potential source of noise laser light hitting the film is the multiple reflections inside the dispersing lens. Of the ≤ 10 J going through this lens, only 36 μJ is intended to hit the film (area = 40 cm^2) as the reference beam. Any of this intense laser light multiple reflected in the dispersing lens and hitting the film would add to the exposure and must be counted as noise, because it is not part of the point source beam used to construct the hologram. To prevent this, the dispersing lens was designed to function also as the Bubble Chamber pressure window, eliminating two potentially reflecting surfaces; the shape of all the dispersing lens surfaces were carefully adjusted, with the aid of a ray tracing program, to make serious multiple reflections miss the film; light absorbing baffles were
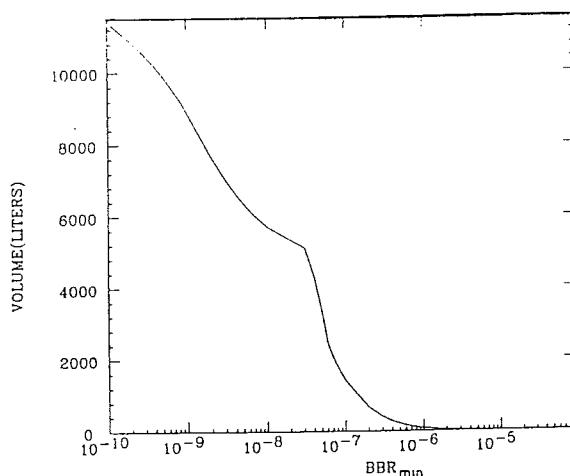
Fig. 4. Visible volume versus minimum detectable BBR in case no noise light is reaching the holographic emulsion.

placed between the lens elements and finally the surfaces in the laser beam were 'V'-antireflection-coated (sections 3.2 and 3.3).

When the Bubble Chamber was sensitive, the intense laser beam near the dispersing lens could induce bubble formation. Later in the laser pulse, these bubbles had grown large enough to scatter significant illumination light directly onto the film, becoming another source of noise laser light. Since this "microboiling" depends on the amount of microscopic particles (N_2 and H_2O) suspended in the Bubble Chamber liquid, this source of noise laser light proved very hard to control, and is thought to be responsible for much of the variation in hologram quality throughout the run. In order to reduce the laser beam intensity where it entered the Bubble Chamber liquid, the dispersing lens was designed so the output beam almost filled the 20-cm diameter of the lens (section 3.6).

2.2. Effects of bubble growth and movement, and vibrations during the laser pulse

As will be discussed in section 4.2, the need to prevent boiling of the Bubble Chamber liquid by the incident laser energy (≤ 10 J) necessitates the use of a "stretched" laser pulse (≥ 1 μs), rather than the more normally used Q-switched pulse (~ 30 ns), in order to minimize the instantaneous power flux in the pulse. This meant that, in principle, the effects of bubble growth and movement and of mechanical vibrations could cause a significant path length difference change between the reference and object beams during the laser pulse. The resulting changing phase between the two amplitudes reduces I_x and increases I_m giving a lower fringe modulation. We assume the phase changes linearly with time during the laser pulse, and we consider the desired "square wave" (i.e. intensity constant with time) laser pulse. Rewriting I_x (from the previous section) to include a phase angle β between E_r and E_b (where β varies during the duration of the laser pulse) $\Delta P/\lambda$ = instantaneous path length difference/wavelength,

$$\beta = 2\pi \Delta P/\lambda,$$

$$I_x = E_r^2 + 2E_r E_b \cos \beta.$$

I_x is then integrated over β from $-\delta$ to δ, choosing a central value of $\beta = 0$ to give the maximum intensity:

$$\bar{I}_x = E_r^2 + 2E_r E_b (\sin \delta)/\delta,$$

with a total path length difference change ($\Delta P/\lambda$) equal to δ/π from the beginning to the end of the laser pulse.

After I_m has been calculated in a similar manner, we find the fringe modulation

$$M' = 2r(\sin \delta)/\delta$$

has been multiplied by a factor $(\sin \delta)/\delta$, which is less than or equal to 1.0. Defining BBR' $(= r'^2)$ as the Beam Branching Ratio needed, with path difference change, to get the same fringe modulation as was obtained without this change:

$$M' = M,$$

$$2r'(\sin \delta)/\delta = 2r,$$

$$r' = r/(\sin \delta/\delta), \quad \text{or}$$

$$\text{BBR}' = \text{BBR}/(\sin \delta/\delta)^2.$$

For a path length difference change of $1/4\lambda$ ($\delta = \pi/4$), we require 1.23 times the BBR to get the same fringe modulation as we had without the change; this is a barely acceptable upper limit. If the change is limited to $1/8\lambda$, the factor is only 1.05 times the BBR.

Bubble diameters D grow according to $D = 2A\sqrt{t}$, where t is the time since growth started and A is a constant depending on the operating conditions (see section 4.2 for details). Assuming the Chamber is operated to grow our desired 100-μm bubbles in 1 ms, the bubble diameter is then growing at a rate of 0.1 μm/μs.

The optical path difference change for light scattered at an angle α off a bubble which has grown in diameter by ΔD is shown in fig. 5. For light which reflects off the bubble:

$$\Delta P = \Delta D n_1 \sin(\alpha/2),$$

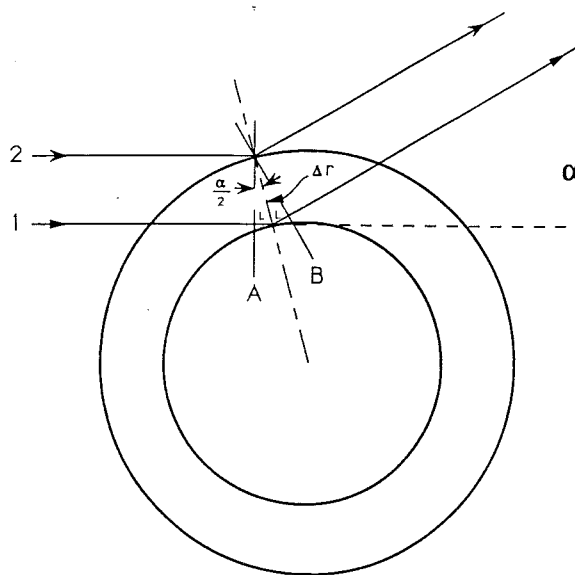where $n_1 = 1.088$ = refractive index of liquid Ne/H_2.

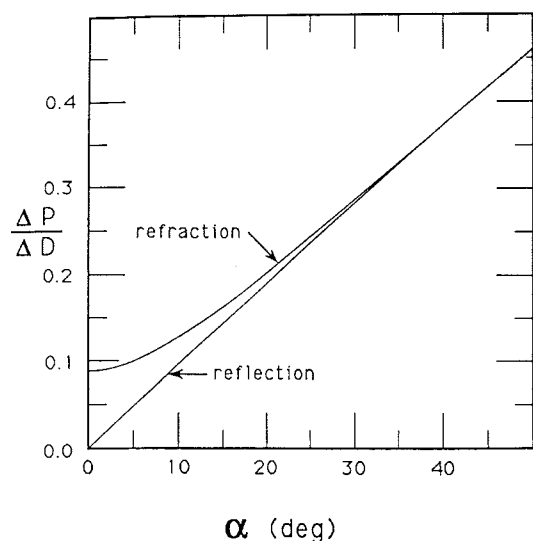Fig. 5. Optical path difference of growing bubble (schematic).

Fig. 6. Change in optical path length per change in diameter for a growing gas bubble in neon–hydrogen (liquid optical index 1.088) as a function of scattering angle α, for both refracted and reflected rays.

The expression for light refracting through the bubble is more complicated and will not be given here, but its value is shown in fig. 6 and agrees with the above expression within 5% for $\alpha > 23°$.

For a bubble with its diameter growing at 0.1 μm/μs, at an α of 30° (45°), the path difference change will be $1/4\lambda$ for a laser pulse length of 12.3 (8.3) μs. Laser pulse lengths of half these values would be required to limit the change in path length difference to the more desirable $1/8\lambda$.

During the first physics run, before this calculation had been made, most of the holograms were taken with 40-μs laser pulses and with higher bubble growth rates. This unfortunate choice clearly extracted a heavy penalty, both in the quality and in the volume of the Chamber that could be recorded in those holograms [11]. Laser pulse lengths of 7.5 μs or less were used during the second physics run.

Motion of the bubbles during the laser pulse has an effect similar to bubble growth. Track and bubble movement can be subdivided into two main categories: in their displacement together with the liquid due to its compressibility during expansion and recompression, and relative to the surrounding liquid, mainly due to buoyancy forces.

– The isentropic compressibility of our neon/hydrogen mixture is 1×10^{-3} cm^2 kg^{-1} [18]. The expansion ratio is $\Delta V/V \simeq 0.6\%$, V being the total liquid volume. The bubble movement together with the liquid is a function of the distance from the piston: it is more pronounced near the bottom of the Chamber than near the top. Furthermore, it depends upon the time when the tracks are produced: before the piston reaches its lowest position during expansion this displacement will be downwards, and during the recompression upwards. Since the beam is injected during the pressure minimum, when the piston is at its lowest position and almost at rest, we can neglect the bubble movement together with the liquid.

– Theoretical predictions of the lift velocity of a bubble show only a slight dependence on temperature in the

$$\Delta P = 2 d n_L \sin(\alpha / 2)$$

displacement d along bisector

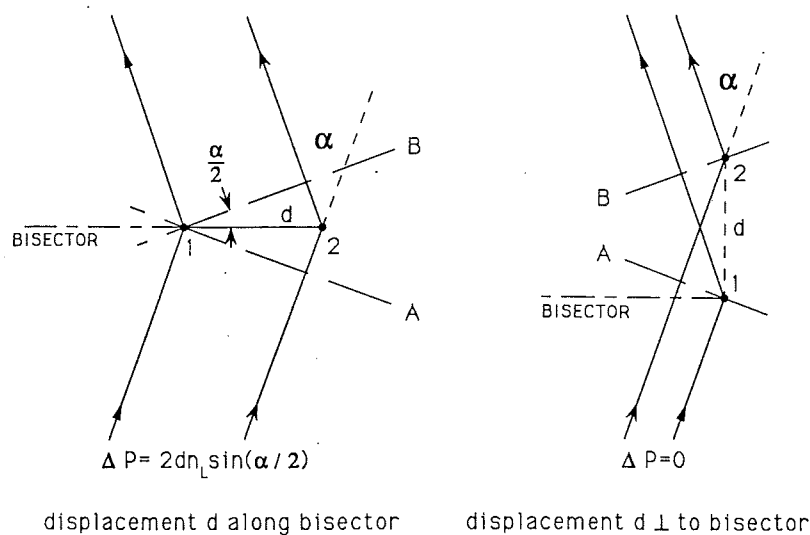$$\Delta P = 0$$

displacement d ⊥ to bisector

Fig. 7. Optical path difference change of moving bubble.

operating range of bubble chambers, but a strong dependence on the actual bubble diameter. A change of speed occurs when a diameter of $D \sim 0.2$ mm is reached during the growth (or recompression) process, i.e. when laminar flow turns into turbulent flow (or vice versa). Measurements had been made in liquid hydrogen in the condition of turbulent flow and gave a constant value of ≤ 20 cm/s, in good agreement with the theory [19]. For our liquid mixture we expect values of the same order. Bubbles to be photographed with holography will have attained, however, only diameters of 0.1–0.2 mm. Therefore, we still have laminar flow and the lift velocity of bubbles is expected to be proportional to their diameter squared: 1–3 cm/s, respectively.

The change in optical path difference for light scattered at an angle α off a bubble which has moved during the laser pulse is shown in fig. 7. Only the component d of bubble motion which is along the bisector of the incoming and the scattered light rays contributes a path difference change; motion in the orthogonal directions contributes no change:

$$\Delta P = 2d \sin(\alpha/2).$$

For a bubble moving along the bisector with a speed of 0.03 μm/μs, at an angle α of 30° (45°), the path length difference change will be $1/4\lambda$ for a laser pulse length of 11.2 (7.6) μs. Laser pulse lengths of half these values would be required to limit the change in path length difference to the more desirable $1/8\lambda$. Most bubbles will have only a fraction of their velocity along this direction; if the motion directions were random, the average of the absolute value of the projection along this axis would be half of the speed.

If the bubble motion is upward, due to buoyancy, the magnitude of the effect will vary in different regions of the holographic volume. In our experiment, the laser axis (i.e. the direction of the reference beam through the Chamber), was inclined at an angle $\beta = 56.2°$ with the horizontal. We define an azimuthal angle γ about this axis with $\gamma = 0$ in the horizontal direction. In the holographic midplane, $d = z \cos \beta \sin \gamma$, where $\cos \beta = 0.56$ and z is the upward bubble displacement. Bubbles exactly to the left or right will not be affected, those above or below the axis will have the largest effect. Nearer the film than the midplane, the effect becomes even larger for bubbles above the axis and less for those below; the reverse is true for bubbles on the dispersing lens side of the midplane.

Vibrations of the dispersing lens and holographic film are induced when the Bubble Chamber is expanded to drop the pressure in order to make the fluid track sensitive. No actual measurements of the vibrations of these components were made during these physics runs, but previous experience indicates that accelerations were less than 5 g and displacements less than 0.1 cm. With these limits, the maximum velocity would be 22 cm/s at a frequency of 35 Hz. Even though this velocity was reached at some time during the expansion cycle, the velocity at the instant the hologram was taken would likely be only a small fraction of the maximum.

If the dispersing lens moves a distance ϵ perpendicular to the laser axis, the reference beam path length does not change. The object beam path length to a bubble at an angle Θ with the laser axis, as viewed from the lens, will change by $\epsilon \sin \Theta$. If the motion is along the axis, the reference beam path length changes by ϵ. The object beam path length will change by $\epsilon \cos \Theta$, giving a net change in path difference of $\epsilon(1 - \cos \Theta)$. Similar expressions hold for motions of the holographic film, except the angle is now φ, the angle of the bubble with the axis as viewed from the film. Since these angles are limited to 30° or less in our application, the perpendicular displacements produce larger path difference changes.

For motion of the dispersing lens perpendicular to the laser axis with a speed of 0.22 μm/μs, at an angle Θ of 15° (30°), the path difference change will be $1/4\lambda$ for a laser pulse length of 3.0 (1.6) μs. However, these pulse lengths are unduly restrictive, both because the maximum velocity is unlikely to occur at the instant of taking the hologram and because the actual vibrations are probably less than the maximum estimate made above.

All three of these effects (bubble growth, bubble motion, and vibration) generally increase in magnitude as the scattering angle α increases. For the first two effects and for the effect of vibrations on bubbles in the holographic midplane the variation is as $\sin(\alpha/2)$, vibrations on bubbles out of the midplane show an approximate $\sin(\alpha/2)$ dependence. Since the light scattered from a bubble decreases rapidly as α increases, the BBR and fringe modulation are already low for bubbles at large α. Usually a good hologram can still be made of bubbles at smaller α, because these effects are smaller and these bubbles started with a higher BBR and more "reserve" fringe modulation. A measurement of the holographic volume is needed to judge the magnitude of these optical path length change effects.

The main parameter available to reduce these effects is to shorten the laser pulse length. This must be balanced against the occurrence of laser-induced boiling (section 4.2), which is reduced by increasing the laser pulse length. Since none of these effects (especially vibrations), nor laser-induced microboiling are well understood, the best compromise laser pulse length must be determined experimentally. Also, the temporal shape of the laser pulse should be as close to "square wave" as possible, in order to reduce the instantaneous power of the beam.

2.3. Laser light distribution in the Bubble Chamber

Our goal was to view the interaction point of high-energy neutrinos in the Bubble Chamber with high resolution in order to study particles with short lifetimes which decay within a few millimeters. While the geometric cross section of the neutrino beam is larger than the diameter of the Chamber, and while events could occur anywhere within the 28-m³ visible volume, the events are more concentrated near the center of the Chamber. To properly analyze these events in the conventional pictures, we only accept interactions with their vertex inside a restricted "fiducial volume" of ~ 12 m³. The main reason for restricting this volume is to allow sufficient track length for the interaction products in the visible volume to accurately measure angles and momenta.

While we would like to record as much of this fiducial volume in the hologram as possible, there are practical limits. The amount of light scattered by a bubble drops steeply as the scattering angle α increases ([17] and fig. 3), requiring more and more laser light to record bubbles with large α. Laser-induced boiling gives the first limit on how much light can be sent to the Chamber, but the limit of total light available from a pulse-stretched holographic ruby laser with present technology is not far behind. More sensitive high-resolution fine-grain holographic film would be a solution, but the Agfa–Gevaert 10E75, pushed by developing with phenidone, is already the most sensitive available on today's market. Sending more light into the Chamber also places a heavier burden on the light absorbing baffles and reflection prevention design of the dispersing lens, as discussed in section 2.1.

We decided to limit the illumination half-angle Θ to 30° from the laser axis, with a reference beam of 0.9 μJ/cm² (needed to expose adequately our film). To find the optimum light distribution from the lens, a computer program was used which divided the field into 1/2° Θ bins, and then added energy to the bin where the least amount of energy would make the next small volume element (0.25 l) of the fiducial volume visible. A BBR of 0.33×10^{-7} was used to define when the volume element would become visible in the hologram (sections 3.3 and 4.10).

The preliminary designs, for a limited laser energy, had given light distributions which rose continuously to a maximum value at a high Θ, and then dropped off. Laser-induced boiling from such a distribution in the Chamber is a *hollow* cone [6], with the whole outline of the cone obscured in the conventional photographs, even though there is little boiling in the central part of the cone. We then investigated distributions with a constant limit on the light intensity. Such distributions would give a solid, but shorter, cone of boiling, thus reducing the obscured area in the conventional photo-

Table 1
Limited and unlimited illumination ($\Theta_{max} = 30°$)

Laser energy [J]	Maximum intensity [J/sr]	Visible volume [l]
10.0	13.0 (limited)	4694
10.0	16.3 (unlimited)	4719
20.0	67.1 (unlimited)	5020

graphs. The results for limited and unlimited illumination are shown in table 1.

We selected the first design (fig. 8) to limit the boiling cone and because very little visible volume was gained by increasing the energy above 10 J, which was also the expected upper limit for a good holographic beam from our pulse-stretched ruby laser.

At the time this light distribution was designed, the effect of boiling within the duration of the laser pulse (the microboiling effect, section 4.4) had not been proven, and so was not considered in the optimization. In the selected design, the light distribution with illumination angle 5° < Θ < 15° is most effective at producing microboiling.

Microboiling affects mainly the reference beam, and thereby the quality of the hologram. To circumvent this effect, a two-beam technique could be envisaged. In such a setup both the light passing through the central part of the dispersing lens and noise light from microboiling must be prevented from reaching the film and the reference beam is derived directly from the laser. Depending on the energy needed, the latter would be taken out by a beam splitter after one of the amplifiers
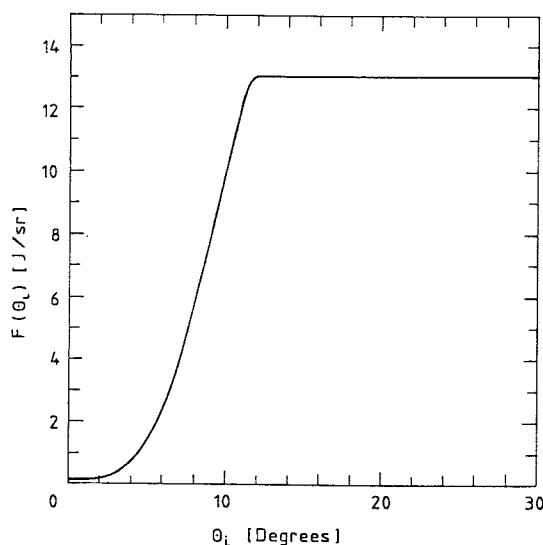
Fig. 8. Design values of the illumination intensity $F(\Theta_i)$ per solid angle as function of the illumination angle Θ_i for the dispersing lens used in the second physics run.
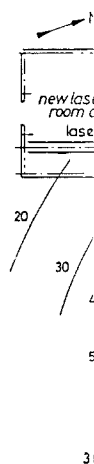
and then directed onto the film. Some technical aspects of such a system have been studied [16], but such development is arrested at present.

3. The experimental arrangement

The layout for the laser beam is shown in fig. 9 (top view). The safety requirements for the operation of non-explosion-proofed electrical equipment near a hy-drogen area, the stray field from the Bubble Chamber magnet and the demand for a dust-free environment made it necessary to install the laser far away ($\sim$ 29 m) from the volume to be holographed. The laser was placed in a separate, air-conditioned clean room. The beam was guided through an evacuated underground pipe to the bottom of the Chamber, where it was made to diverge by the dispersing lens. The aspheric lens was positioned in the Bubble Chamber vessel, its flat side facing the cryogenic liquid (Ne/H_2 at $\sim$ 30 K). It also acted as a pressure window. A ruby laser was used because its wavelength does not overlap too much with the spectrum of the flash lamp of the conventional cameras, and also because of the availability of a high-quality ruby laser specifically designed for holographic purposes. A description of the various elements follows.

3.1. The laser

Originally a KORAD laser [20] had been used (available during our tests for no charge), but was replaced

Fig. 9. Laser room, beam pipes, and Bubble Chamber (top view). Shown are lines of constant magnetic field near the laser room.

for the physics runs by a powerful holographic ruby laser system (JK Laser System 2000). Our main modification of this commercial system consisted in incorporating a pulse stretching circuit into the oscillator stage. Its latest version has been described in refs. [21,22]. The characteristics of the light output obtained were:
- Pulse duration adjustable from $\sim$ 2 to 100 μs, but studied in more detail in the range from 3 to 16 μs,
- fairly flat pulses with little overswing at the beginning,
- coherence length in excess of 11 m for $\sim$ 2-μs pulses,
- maximum energy varying with these conditions, but < 8 J with a stability of $\pm$10%,
- repetition rate for the above conditions: $\sim$ 1 pulse every 10 s with reproducible pulse shapes.

Precautions had to be taken to prevent adverse effects on the temporal output characteristics of the amplified laser beam by a) specular and diffuse reflections of downstream optical elements, which can gain energy by passing through the amplifiers, and b) self-oscillation between the laser amplifiers. Both effects would disturb the correct performance of the oscillator pulse stretching circuit.

These problems could be solved by placing an optical isolator between the amplifiers and the oscillator. The light from the oscillator has a linear vertical polarization and the amplifier rods were aligned for this polarization. This isolator must not alter the polarization of light going from the oscillator to the amplifiers. But the plane of polarization of light travelling in the opposite direction should be rotated by 90° in order to discriminate between the back-reflected light and the light coming from the oscillator. Such a system was built using a polarizer, a Faraday rotator (aperture 5 mm, optimum spectrum between 500 and 800 nm, forward transmission of $\sim$ 85%, and minimum reverse isolation of 100:1, Manufacturer: Optics for Research, Inc.) and a half-wave plate.

3.2. The beam transport and monitoring

The output beam of the laser was sent down by a mirror, and it traveled underground in a 30-cm diameter beam pipe with three bends and a total length of $\sim$ 27 m. The pipe was closed at both ends by flat windows. Three mirrors inside the pipe directed the beam towards the Bubble Chamber. The system was kept under vacuum, both to avoid back reflections from focusing the laser beam in a medium, and for safety and cleanliness.

Special mounts were designed to allow for the adjustment of the mirrors while the system was under vacuum. Front surface dielectric-coated high-reflectivity mirrors were used in all four locations. Once inside the Bubble Chamber building, the laser beam pipe was reduced to 15 cm in diameter, which was adequate for
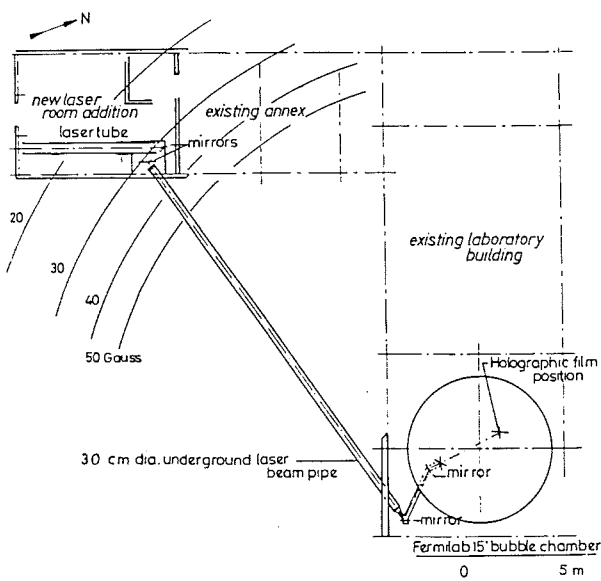
the 5-cm laser beam and dispersing lens diameter. The laser beam was increased to ~ 8 cm in diameter during the second physics run.

In order to obtain a spatial distribution of laser light on the dispersing lens of good quality, we designed and installed an optical relay in the beam pipe. An optical relay is intended to transfer a beam of light from one plane to another, maintaining both the position, angles and phases of all rays. The basic relay is two positive lenses of focal length f, separated by a distance $2f$. Light from a plane on one side of these lenses will be relayed to a plane on the other side, provided the two planes are a distance $4f$ apart. We generalized this to include a magnification change between the planes, both to expand our laser beam (~ 2-cm output at the amplifier) to the 5-cm diameter needed and to help remove the need for any relay lenses within the virtually inaccesible 19-m underground section of our existing laser beam pipe.

A two-stage relay was used. The first stage used the existing JK Laser lenses, modified only by reversing the two telescope lenses so that the positive lens was now closer to the laser, and relayed a plane at the output of the oscillator, through the amplifiers, to a plane at the output of the telescope. The focus (required in each relay stage) was at the spatial filter. This could be done in air, because only the low power laser beam from the oscillator was present at this point. The second stage relayed this plane to the input of the dispersing lens.

The focus of this second stage was in the underground beam pipe and has the full laser power. At this focus, it is essential to have vacuum (~ 0.1 Torr), since high beam intensity in air results in plasma formation with a harmful back reflection of the beam. We experienced such damage during initial tests with the beam-expanding telescope.

The lenses for the second stage relay were telephoto combinations, where a strong positive and a strong negative lens act together to produce the same effect as a weaker positive lens some distance away. The telephoto combination ($f_n = -0.35$ m, $f_p = +0.6$ m) mounted just outside the laser end of the underground section of beam pipe functioned optically as if it were a weaker positive lens ($f = +3$ m) mounted 3 m further into the pipe. These BK7 lenses were available commercially and then 'V'-coated for the ruby wavelength. Finally, the distance between the lenses in the combination was adjusted to correct for the actual focal length of the lenses.

The first lens in this combination was mounted outside the evacuated beam pipe and could be adjusted to vary the size of the laser beam at the dispersing lens, while still maintaining an acceptable approximation to the relay condition. The other second stage relay lenses were mounted inside the vacuum pipe, near the ends of the underground section.

The detailed design and final optimization of the two-stage relay system was done using Code V *. This program was also used to trace reflections from each lens surface backward through the relay to learn if any were focused near optical elements or the laser. One such potentially damaging back reflection was found; it was steered to miss the mirror at risk by a small tilt off-axis of the second lens in the first combination. This two-stage relay greatly improved the spatial distribution of the laser beam on the dispersing lens; it is discussed in ref. [23].

Modifications for holography had to be made on the bottom part of the 15-Foot Bubble Chamber, as shown in fig. 1. The laser beam entered its vacuum tank through a warm window to reach the Chamber window and the dispersing lens assembly. Since the main vacuum tank is pumped by oil diffusion pumps, a pipe had to isolate the optic elements to prevent oil contamination and contain the Chamber liquid in case of the unlikely breakage of two pressure windows. The spaces between the dispersing lens, which served as Chamber window, the safety window, and the vacuum tank window were pumped by the same high-quality, clean (ion getter) pumps that serviced the six sets of hemispherical fisheye windows at the top of the Bubble Chamber.

For protection against the remote possibility of breaking or leaking of all three pressure windows, which would allow the escape of the Bubble Chamber liquid, this pipe was equipped with an automatic valve just outside the vacuum tank. The pipe contained a bellows to allow for movement of the Bubble Chamber vessel relative to the vacuum tank during cooldown and during the expansion cycle.

All transparent elements in the laser beam path to the Bubble Chamber (i.e. four windows, the dispersing lens plus a small negative lens) were made from fused silica of optical grade Homosil. This material has an extremely small coefficient of thermal contraction, excellent homogeneity, and a very high threshold for damage from the high-power laser beam (≥ 1.3 GW/cm^2). In our experiment the beam was spread over a surface area of ~ 20 cm^2 on most of the lenses, and, with the laser operated in the pulse-stretched mode described in section 3.1 above, an ample safety margin against laser damage was maintained.

3.3. The dispersing lens

During the initial part of the experiment a single element dispersing lens was used. It had been tested earlier in BEBC [6.24] and was designed for a parallel, 5 cm in diameter Gaussian-distributed beam from a ruby

---

* Optical design ray tracing program leased from Optical Research Associates, Pasadena CA, USA.

laser. It dispersed the light over a cone with a half angle of ~ 28° within the Bubble Chamber's visible volume. It was mounted in the vacuum space between the flat Chamber and vacuum tank windows, and could be moved along the optical axis to allow for the study of laser-induced boiling as a function of the peak power density at the entry of the beam into the liquid.

For the second physics run we used a new, two-element lens (quartz: optical grade Homosil), which served also as Bubble Chamber window.

The lens was designed so as to minimize boiling on the quartz-liquid interface:

a) the laser beam intensity was spread over a larger surface as compared to the one-element lens (315 and 125 cm^2, respectively);

b) the flat output surface was inclined by 34° from horizontal (as was the Chamber window for the one-element lens), which reduced the possibility of accumulation of "dirt" on this surface; and

c) the mounting flange was now underneath the lens surface to avoid trapping of parasitic bubbles (fig. 10).

The combined dispersing lens/Bubble Chamber window system was designed under several constraints. It was required to disperse a parallel incident beam of diameter 5 cm to fill a cone of half angle 30° in the Bubble Chamber liquid. The incident intensity distribution, assumed to be uniform after propagation of the beam from the laser 29 m away, was to be transformed into the calculated optimum angular intensity distribution in the Chamber. The surface energy density as the beam entered the liquid was required to be < 0.1 J/cm^2 to prevent boiling. There should be no significant peaks in the light intensity due to reflections of the beam from the lens surfaces. Finally, the center of the lens system was required to have a focal length determined by the requirement that the reference beam exposes the film correctly.

In order to achieve the large beam diameter at the quartz–liquid interface a system of two lenses with intervening drift space was utilized. For ease of manufacture, the first lens was plano-concave with a standard radius for the concave surface. A first design of the second lens/window resulted in a surface contacting the
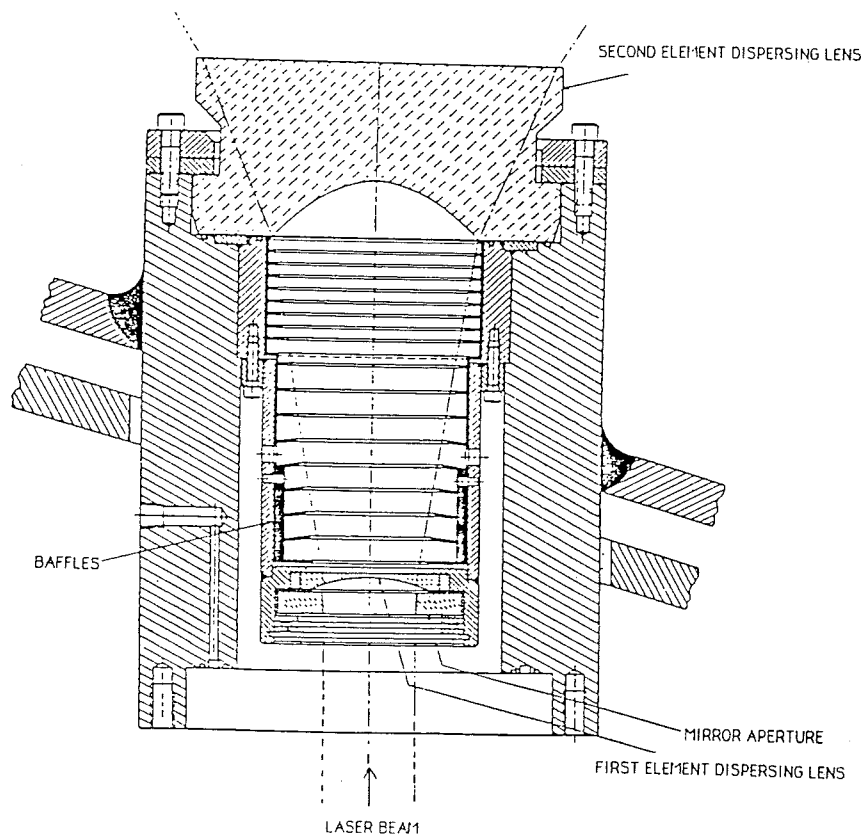

Fig. 10. Drawing of the dispersing lens, with the baffles between the two lens elements.

liquid that was not quite plano. Since this design would have required grinding and polishing two optical surfaces with accurate control of their concentricity, it was decided to constrain the second surface of this lens to be plano also.

The actual design of the aspheric first surface of the lens/window was performed numerically. Starting from the center, rays of increasing input beam radius were traced through the plano-concave lens. The integrated laser energy inside each ray was calculated using the assumed flat input beam distribution. The required outgoing energy distribution in the Bubble Chamber liquid was also integrated to produce a table of total energy contained within various angles. This table was entered with the integrated incident beam energy and the desired outgoing angle was determined. Using Snell's law, this angle was propagated back through the quartz–liquid surface to determine the angle of the ray within the quartz.

Using the angles of the upcoming ray from the plano-concave lens and the outgoing ray within the quartz as determined by back propagation, Snell's law determined the slope of the aspheric surface. The series of slopes thus determined by tracing rays of increasing radius was integrated to yield the shape of the aspheric surface. Finally, the inner 0.7 mm of the calculated surface was modified to be spherical with a radius of 5.283 mm determined by the requirement that the central portion of the beam covers an output half angle to $1.6°$ and a circle at the film (4.1 m away) of radius 11 cm.

This was chosen to be three times larger than the film size to allow for misalignment. It produces the required beam intensity for correct exposure.

Fig. 10 shows the lens combination and the baffles between the two components. The latter are intended to catch the light from the antireflection-coated surfaces of the first lens and the inner surface of the aspheric lens, as well as reflections from any other parts of the assembly, which would otherwise spoil the reference beam.

As pointed out earlier, multiple reflections inside the dispersing lens are a potential source of noise light which would increase the minimum detected BBR and greatly reduce the holograph volume. A computer program was written to trace all reflected rays through the optical system shown in fig. 10. The program kept track of the energy in both S and P polarization for the ray and divided these energies into the reflected and transmitted rays at each optical surface, according to the coating assumed. Laser energy leaving the system from the various surfaces was histogramed and individual ray paths could be printed. Detailed information for rays hitting the film was output. For these calculations, the holographic film was taken to be a 3-cm radius circle on the lens axis, 400 cm above the lower edge of the lens. The energy of the design reference beam in this circle is 26 μJ.

Consider the reflected rays shown in fig. 11a for an early design of the dispersing lens with uncoated surfaces. (To save figure space, two rays are shown, one on each side of the figure; in fact, both rays are cylin-
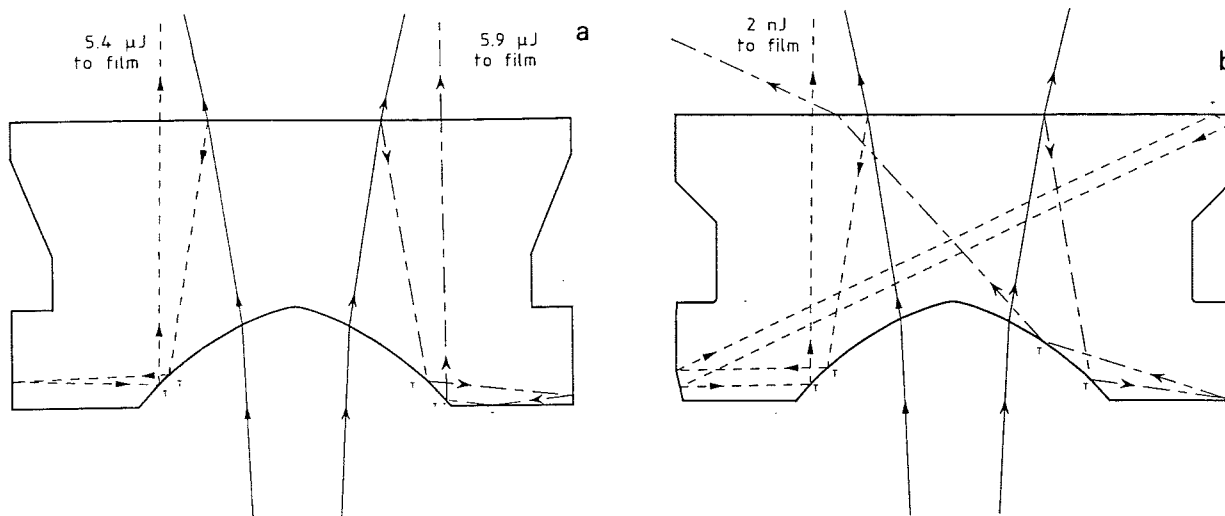

Fig. 11. (a) Paths of two light rays (with slightly different initial radial position in the laser beam) through an early design of the dispersing lens. The main rays are shown by solid lines; reflected rays by dashed lines. A "T" indicates a total internal reflection. The total energy reaching the film, from the bundle of reflected rays similar to the one shown, is also given, assuming uncoated lens surfaces. (b) Paths of two light rays (chosen to be the worst remaining cases, similar to the two rays in (a) above) through the final design of the dispersing lens. As the result of tapering the lower sidewall of the lens, the ray starting on the left undergoes two additional (nontotal internal) reflections before reaching the film with greatly reduced energy. Reflections from the ray starting on the right now miss the film entirely. Uncoated surfaces were also assumed here.

drically symmetric.) If this design had been used 11.3 μJ from these two reflections alone would have produced an average noise to total light intensity ratio of $11.3/37.3 = 0.3$, which would have doubled the minimum detectable BBR (fig. 20), and drastically reduced the volume of the Chamber visible in the holograms (fig. 4). This noise light can be reduced by either applying a high quality antireflective coating to the optical surfaces or redesigning the lens to prevent the reflected rays from reaching the film. We elected to do both.

Similar rays (actually the new worst case rays were selected) are shown in fig. 11b for the final lens design. Tapering the lower sidewall of the lens has reduced reflections from the ray starting on the left to an insignificant level, even with uncoated surfaces, and caused reflections from the ray starting on the right to miss the film completely. The other shape changes to the lens sides similarly reduced reflections from rays starting from different radial positions. After making all design shape changes, an exhaustive ray tracing check was made with the computer program to be sure that solving known reflection problems had not created new ones.

The effect of antireflective coating on the principle (aspheric and top flat) surfaces of the dispersing lens was also investigated with the ray tracing program. (The cylindrical side surfaces of the 20-cm diameter lens would have been too difficult to coat.) Using a single layer magnesium fluoride coating would have reduced the 11.3 μJ of fig. 11a to 6.2 μJ hitting the film. This rather small effect is because of the rather low optical index of fused silica (1.455) compared to MnF_2 (1.38). The three-layer V-coating for the ruby laser wavelength actually used was calculated to reduce the energy of fig. 11a to 0.19 μJ.

A good antireflective coating is also very important in reducing diffuse reflections. With uncoated surfaces, almost 0.3-J reflected light goes out the dispersing lens sides and bottom flat. Most of this light encountered the back (carbon filled) teflon lining of the lens mount, but some fraction is diffusely reflected back through the lens into the Chamber, contributing to the level of the noise light. The three-layer V-coating reduces this by a factor of ~ 50.

3.4. The 15-Foot Bubble Chamber

The 15-Foot Bubble Chamber is an almost spherical vessel (fig. 1), 12.5 ft in diameter [25] *, operated with cryogenic liquids. Its total volume is about 33 m³, the visible volume is limited by the optics to some 28 m³. It can be photographed simultaneously by six cameras arranged on the top. These cameras have wide-angle lenses, each of which sees through three concentric hemispherical windows, so-called fish-eye lenses, into the liquid. Conventional photography is made in bright-field illumination, using an annular flashtube around each wide-angle lens. The inside of the Chamber is wall-papered with a retrodirective material (Scotchlite), which has the property of returning incoming light parallel (with a small opening angle of only $\sim 0.5°$) to the lens, almost independent of the angle of incidence up to 60°. Optionally, the camera ports can be equipped with a lens about 2.5 times the resolution of the standard lenses, but, with a considerably smaller volume (~ 1 m³) in focus. For our experiment such a lens was put into one optic port. Another port was used for the holographic camera.

The Chamber has on its bottom a large expansion piston (1.8 m in diameter) to sensitize the liquid during the arrival of the pulsed particle beam. For optical reasons this piston is covered by a floating disc (2 m in diameter) covered with Scotchlite. During our runs the expansion sequence was three pulses at 10-s intervals, followed by a 40-s pause. It was determined mainly by the three fast ejections of protons from the Tevatron during the flat top of one acceleration cycle of ~ 60 s.

For thermal insulation the Chamber vessel is surrounded by a vacuum tank, which also contains the two superconducting coils with their cryostat, producing a magnetic field of 3 T.

The Bubble Chamber is surrounded by electronic detectors, one being installed inside the vacuum tank between the liquid vessel and the magnet, covering almost 360° (Internal Picket Fence, IPF [26]), and counter planes downstream, outside the vacuum tank (External Muon Identifier, EMI [27]).

3.5. The holographic camera

The new laser window on the bottom of the Bubble Chamber aimed directly at one of the optic ports. An existing camera was modified such that the holographic film was transported down to the center of the fish-eye lenses 4.1 m away form the dispersing lens. The film was positioned in the fish-eye such that its plane contained the center of curvature of the fish-eye and was perpendicular to the reference beam direction to within about 1°. The film drive was modified to handle the stiffer (thicker) holographic film used during part of the run. The new platen was lapped flat to $\lambda/4$ and a new vacuum system was added to securely clamp the film. Three platen-based fiducials were exposed on the holographic film to permit accurate placement of the film on a replay machine. A red colour filter (RG 665) was installed in front of the holographic film as well as filters with a complementary colour (BG 39) in front of the flashtubes of the conventional cameras in the other

---

* The beam entrance cone had been removed, which originally extended the chamber's length in the beam direction to 15 ft.

ports. These filters prevented light from the conventional cameras from exposing the holographic film. Exposure of the conventional film by laser light was not a problem at the present energy level, due to the high f number of the conventional lenses ($f/12$), the presence of a Wratten 58 colour filter in each lens, and the low sensitivity of the Kodak 2482 film to the deep red ruby laser light. Four fast photodiodes were mounted on the platen next to the holographic film to monitor the reference beam intensity.

3.6. Timing

The exact timing for the firing of the laser with respect to the occurrence of the neutrino interaction is crucial for our holographic recording. The beam spill from the accelerator has a width of ~ 3 ms, and an interaction can occur during this entire interval. However, we needed to determine the interaction time with a precision better than ~ 0.1 ms to be able to record the bubbles from such an event after a growth time of ~ 1 ms, when they obtained the desired diameter of ~ 100 μm (see results in section 4.9). Therefore, we had to rely on the real time information from the coincidence of hits in the electronic counters (event trigger derived from EMI and IPF) outside the active Bubble Chamber volume [28].

A lower limit on the time delay ($\geqq 0.9$ ms) for the laser is given by the inherent features of the laser power supply and the rise time of the flash lamp voltage. The ruby rod contains the maximum energy at ~ 1.1 ms after power is applied to the flash tubes, and at a time less than 1.0 ms the laser output energy is too low to produce good holograms. It was thus necessary to construct a trigger logic to generate a signal immediately after the event occurs. The injection time of the neutrino beam relative to the expansion of the Bubble Chamber, the expansion ratio and the liquid temperature are parameters which allow the adjustment of the growth rate of bubbles. We operate such that 100-μm bubbles are produced after ~ 1 ms for the holograms and ~ 400-μm bubbles after ~ 10 ms for the conventional photographs.

4. Experimental results

Several technical aspects of huge Bubble Chamber holography were investigated and centered around the laser-induced boiling, which affects the usefulness of the conventional photographs and the hologram quality. We studied the effects of:

- alignment, size and spatial distribution of the laser beam in front of the dispersing lens upon visible volume and image quality;

- pulse duration (and energy) upon macroscopic boiling;
- laser-induced microscopic (and other parasitic) bubbles upon the minimum detectable beam branching ratio;
- pulse duration upon picture clarity (vibration of optical elements, liquid turbulence, bubble movement and growth);
- filtering the liquid upon boiling;
- back reflections upon shape of the stretched pulse; and
- operating conditions of the Bubble Chamber (temperature, expanded pressure) upon bubble density and size and upon the visibility of tracks in holograms.

4.1. Laser beam alignment and reflections in the chamber

Preliminary alignment was done by directing a He–Ne laser (7 mW), mounted on the JK Laser support plate, sending its light via two 45° (removable) mirrors down the ruby laser beam path and using ground glass. Initially the alignment, position, and spatial structure of the ruby laser beam were studied by temporarily redirecting the beam out the side of the pipe with a movable mirror just before it entered the dispersing lens and using burn paper. This was later replaced by a more sophisticated system, which monitored the beam profile and its position, angle of incidence on the diverging lens and energy on a pulse-by-pulse basis, using an on-line computer in the Bubble Chamber control room. This system is described in ref. [23].

Warm Chamber tests indicated the necessity of having ~ 6 J of laser light to get the right exposure on the film and to obtain holograms in a reasonably large volume. At this high intensity a large amount of stray light can be produced and must be prevented from reaching the holographic film by multiple reflections. A calculation of the effect of stray light on the holographic fringe modulation on the film has already been given in section 2.1, and the importance of minimizing this effect was treated there.

Baffles were mounted in the Bubble Chamber covering the entire 30° half angle laser illumination cone to absorb as much of the light as possible. Any unabsorbed light will undergo multiple reflections inside the Chamber and a fraction will hit the holographic film, reducing the fringe modulation.

The baffles on the main spherical wall, made out of 220 blades, were arranged somewhat like venetian blinds. They were constructed of black anodized aluminum. The design was such that any ray of laser light would be reflected at least twice by a black anodized surface before reentering the main volume of the Bubble Chamber. Those upper horizontal surfaces that were visible from the conventional cameras were

cover
Chan
Tl
the to
on tl
Becau
need
("no
any
were
Fi
them
was o
12b s
ation
camer
of the
The e
minin

4.2. G

Th
boilin
scopic
scatte

Fig. 12
the six
on th

covered by Scotchlite to minimize the reduction in the Chamber's useful volume.

The baffles in the "beanie", or small hemisphere at the top of the Bubble Chamber were similar to the ones on the main sphere, but differed in several details. Because of the smaller radius of the hemisphere, the need to avoid the cylindrical camera window mounts ("nozzles"), and the need to block the line of sight from any of the six cameras, the 221 beanie baffle blades were mounted in 24 planar segments.

Fig. 12a is a photograph of the baffles (not yet all of them installed in the beanie), taken when the Chamber was open, from the region of the expansion piston. Fig. 12b shows part of the baffles, as seen during the operation of the track-sensitive Chamber with one of the cameras. It shows that parasitic boiling on the borders of the baffles was at a very low and acceptable level. The efforts to reduce stray light from the laser to a minimum were successful, as can be seen from fig. 13.

4.2. General remarks on parasitic (laser-induced) boiling

The study of the pulse stretching upon laser-induced boiling was a main concern. Bubble sizes are "microscopic" (≤ 10 μm) during the laser pulse, but can scatter enough light to dilute the reference beam. The

diameter of these densely packed bubbles increases in proportion to the square root of their growth time, and they are "macroscopic" (~ 100 μm) when the conventional photographs are taken. This will be discussed in more detail in the following sections.

Bubble creation has not been described analytically in a completely satisfactory manner, neither for the so-called parasitic bubbles formed on uneven surfaces, nor for production by ionizing particles (e.g. [29,30] and [30–33], respectively). The main difficulty arises from the insufficient knowledge of the energy deposited within the volume of a critical bubble with a diameter of $\sim 5 \times 10^{-6}$ cm (about 200 eV for heavy liquids), which has to take place within less than 10^{-10} s.

Laser light could ionize hydrogen or neon (ionization energy for liquid hydrogen ~ 20 eV, for neon ~ 130 eV) by a multiphoton process and thus reproduce the usual mechanism for bubble creation; the excitation of the hydrogen molecule could constitute another option. As shown in ref. [34], this possibility was ruled out for the production of bubbles with a nitrogen laser ($\lambda = 337$ nm, 3.68 eV) in an argon, nitrogen, and a hydrogen bubble chamber.

Similar calculations for our experiment, where the thermodynamic conditions of the liquid, the wavelength of the laser ($\lambda = 694$ nm, 1.79 eV), its pulse duration,
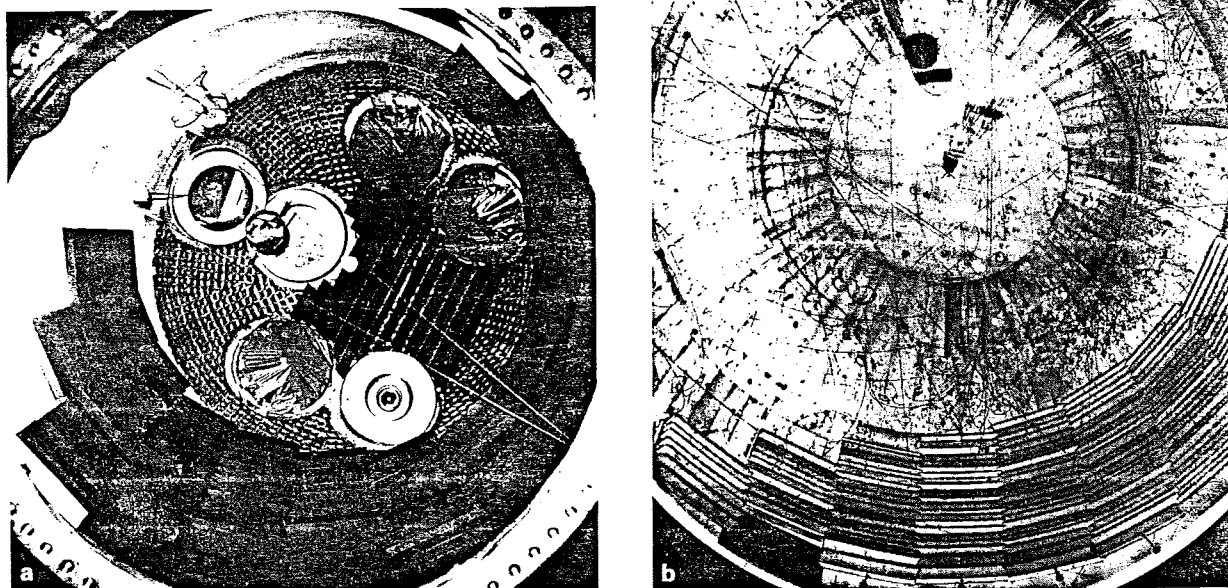

Fig. 12. Baffles inside the Bubble Chamber: (a) view from the piston region towards the top of the empty Bubble Chamber, showing the six optic ports, the rippled structure of the main heat exchanger (beanie head), some of its baffles, as well as most of the baffles on the side walls; (b) view from one of the cameras into the track-sensitive Bubble Chamber, showing the baffles on the side walls.

laser-induced bubbles (number of bubbles per unit volume) to an acceptable level.

During all tests with short pulses, when we produced bubbles abundantly, we found that they did not grow anywhere to sizes comparable to bubbles along particle tracks. A plausible explanation is that they are too densely packed; there is not enough heat available in their vicinity to supply the energy for "normal" growth. It was not possible to determine accurately the diameter of these bubbles:

a) identification of individual bubbles in stereoviews is not possible, and therefore we do not know sufficiently well the spatial coordinates (magnification), and

b) the diameter of the laser-induced bubbles is considerably smaller than the resolution limit of the standard optics (~ 500 μm) [6,11].

An attempt to do this was made by projecting these bubble images on a conventional scanning table with high magnification. The bubble image sizes along the upward edge of the hollow boiling cone were measured as FWHM value of their intensity profile using an array of photodiodes and an oscilloscope. The Bubble Chamber coordinates of the measured points were obtained using two-view reconstruction from which the demagnification of the fish-eye windows and camera lenses were calculated. The proportionality constant A in the bubble growth law was determined, with a fairly large uncertainty, and found to be a factor of ~ 3 smaller than the constant determined for track bubbles [11].

Ideally, one would like to determine, as a function of laser energy and pulse duration, the volume in which laser-induced bubbles appears, as well as its shape. Due to the energy distribution of the laser light given by the design of the dispersing lens used in the first physics run, this cone was hollow (see also ref. [6]). Since the contours of this volume fade out, only estimates could be made.

For the tests in the technical run the height of the boiling cone, measured from the dispersing lens, was assessed. The laser was operated in free-lasing, Q-switched, and stretched-pulse modes. These laser pulses, at various energies, were injected into the track-sensitive Bubble Chamber during its pressure minimum (75/25 mole% Ne/H$_2$ at 30 K (P_{vapour} = 7.8 bar), $P_{chamber}$ = 8.6 bar, $P_{expanded}$ = 5.6 bar). Conventional photographs were taken ~ 10 ms after the laser pulse. Fig. 14 shows photographs for the three kinds of pulses at about the same energy. The height of the boiling cone was found to have a roughly linear increase when plotted against the square root of the incoming laser energy. Fig. 15 shows measurements of the height of the boiling cone versus the incoming laser energy for Q-switched and stretched (~ 2.2 μs) pulses. This plot shows that the height of the boiling cone is proportional to the square root of the total light input energy. This result is con-
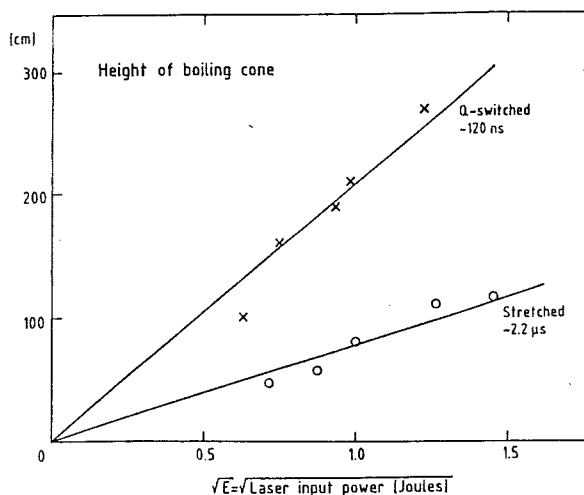

Fig. 15. Height of boiling cone inside the liquid as function of laser input power for two pulse durations.

sistent with theoretical calculations if one assumes a threshold light flux for bubble creation. The pulse-stretched and the Q-switched data are in agreement with a threshold light flux of the order of 100 W/cm^2. This is, however, two orders of magnitude below the flux one would need to explain bubble formation by ionization.

For the same amount of boiling one can increase the laser energy by a factor of ~ 7 by stretching the pulse from 120 ns to 2.2 μs. The boiling is reduced to negligible amount when stretching the pulse to the range of tens of microseconds.

When using the two-element dispersing lens we could send up to 6-J laser pulses with durations as short as 4 μs into the Chamber producing practically no macroscopic boiling. This improved behaviour, as compared to the use of the one-element lens (≤ 0.6 J), was partially due to the decreased energy density of the beam when entering the Chamber liquid, and partially due to the enhanced flatness of the laser pulse.

4.4. Pulse stretching and microscopic boiling

The laser-induced bubble formation and growth during the laser pulse, affects the hologram by scattering additional light into the reference beam, thus reducing the fringe modulation (section 2.1), but it is expected to have very little influence upon the object beam.

There is some indication for the presence of a time threshold for the absorption of sufficient energy on particulate matter, before the first bubbles can be created. After this initial delay bubbles are created on these hot spots during the remainder of (and even beyond) the laser pulse. Their growth rate will follow the $t^{1/2}$-law. Diameters of 4, 12, and 40 μm at the end of the light pulse are calculated for stretched pulses of

1, 10 and 100 μs, respectively, when using the growth factor *A* for track bubbles. These diameters constitute an upper limit, they are probably smaller by a factor of ~ 3 (section 4.3).

Convincing evidence for the presence of microscopic bubbles near the dispersing lens came from the simultaneous measurement of the laser beam intensity behind the last amplifier and at the film platen, and is shown in fig. 16. The quality of the holograms was in general good when the time dependence of the intensity at the two monitors was similar and flat with time. However, the hologram quality degraded and tracks became fuzzy when, for an incoming flat pulse, the intensity at the film platen showed a substantial increase with time. We explain this behaviour by the production of microbubbles, which scatter useless light into the reference beam. Then the lens no longer acts as a point source. The reconstructed holograms of the laser entrance window also indicate the presence of the boiling.

Fig. 17 shows the increasing slope of the light intensity vs time curve, which was used as an on-line monitor for the amount of microboiling, measured at the film platen with increasing laser input energies at a pulse duration of 7.7 μs.

4.5. Filtering of the liquid and boiling

The 15-Foot Bubble Chamber is equipped with a special pump loop cooling circuit. Chamber fluid is withdrawn from the space underneath the piston, cooled, and sent to an external liquid pump through transfer lines. The pump is in an external dewar to remove it from the high magnetic field of the Bubble Chamber. The fluid is then returned to the Chamber in one of two ways. The primary path is through a cooling loop around
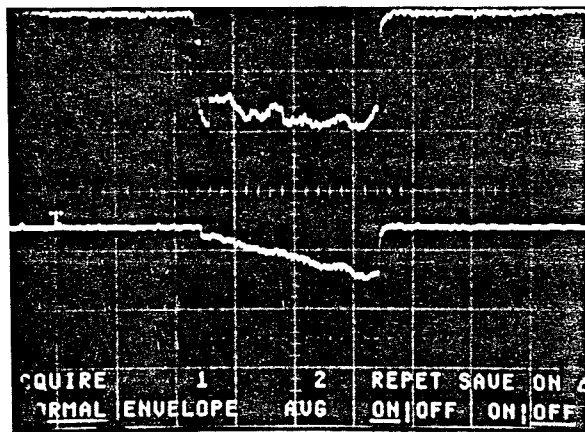

Fig. 16. Oscilloscope picture of light intensities (arbitrary units) of a laser pulse (duration 2 μs) vs time. The upper trace is measured downstream of the last laser amplifier; the lower trace is measured with photodiodes on the film plane. The horizontal scale is 0.5 μs/div.
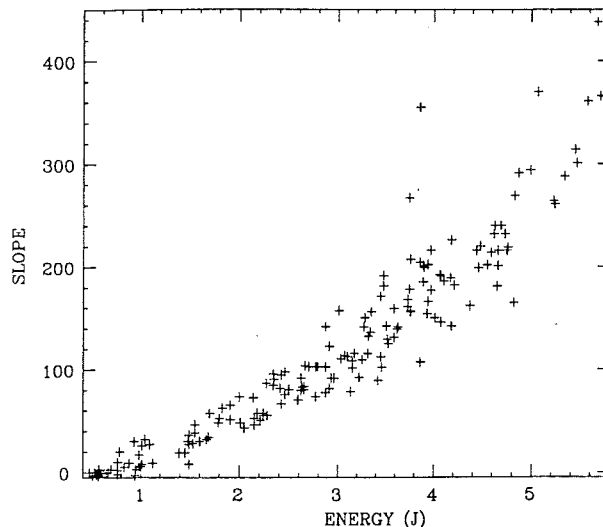

Fig. 17. Slope of the laser light intensity vs time curve measured at the film plane, as function of laser input energies into the Chamber for 7.7-μs pulse duration.

the piston seal area, to remove the heat generated by the sliding piston seals, and then back into the space underneath the piston. An alternate path is to the top of the Bubble Chamber; this mode is frequently used to help mix the part neon, part hydrogen fluid. The necessary piping, valves, and two filter holders were installed at the output of the pump to hold commercially available 5, 2, 0.5, or 0.2-μm sintered metal cryogenic filters. The flow was directed through one filter at a time; the other filter element could be inspected or replaced without stopping pump loop flow. In the mixing mode, a volume equal to the Chamber volume passed through the pump loop and filters about every 10 h. This filtering was done whenever the Chamber was not pulsing.

No pressure drop across the filter was observed during the filtering, and they did not reveal any accumulation of macroscopic solid matter during their inspection at intermediate warm-up. We do not know for sure if filtering actually removed particulate matter from the Chamber liquid and reduced the laser-induced boiling. We are left with various hypotheses:
a) particulate matter is so small, that it can even pass through a 0.2-μm filter;
b) that due to the low viscosity of the liquid these particles were not moved towards the filter;
c) and/or that adhesive (electrostatic) forces attached most of it to the Scotchlite of the Chamber wall and to the dispersing lens.

4.6. Bubble Chamber operating conditions

Once the mixture ratio of neon to hydrogen is chosen for physics reasons (density, absorption, collision

and radiation lengths), the only adjustable parameters are the liquid temperature and the expansion ratio. They must be chosen such as to give optimum bubble size and density ($\geq 50/$cm), both for holography and conventional photographs.

A way to satisfy these requirements simultaneously is to raise the liquid temperature above values generally used in big bubble chambers (figs. 7 and 8 in ref. [33]). However, one then has to accept the (minor) disadvantage that tracks become fairly solid in the conventional photographs due to bubble coalescence. Any ionization measurements for particle identification suffer from this operation mode.

The conditions (temperature of the liquid, pressures, delays for triggering the laser and the flash lamps) used for most of the second physics run were:
62/38 mol% neon/hydrogen;

T_1 (mixture) $= 7.47$ bar $= 108.4$ psia $= 29.6$ K;
$P_{vapour}(H_2$ bulb) $= 7.82$ bar $= 112$ psia;
$P_{chamber}$ $= 8.41$ bar $= 122$ psia;
$P_{expanded}$ $= 5.31$ bar $= 77$ psia;
Δt_{laser} $= 1$ ms;
Δt_{conv} $= 8$ ms.

Our single-beam technique was particularly sensitive to microboiling near the entrance of the laser beam into the liquid. Heat convection inside the Chamber is slow. Once the liquid near the dispersing lens is heated, the following laser pulse(s) will tend to escalate the boiling process due to the now higher sensitivity of the liquid. Therefore, efforts were undertaken to keep the liquid in the lower part of the Chamber cooler by a few hundredth of a degree than on its top. In addition, the pressure drop during expansion could be reduced slightly, so that the desired bubble growth rate and density could be maintained, but the sensitivity of the liquid near the laser entrance was lowered.

It is probable that particulate matter settled on the surface of the dispersing lens and acted as bubble nuclei when hit by the laser beam. Attempts were made with some success to remove this matter by sending a few Q-switched laser pulses of high energy into the Chamber, thereby producing violent boiling and large convection to wash the dirt away.

4.7. Holographic film material and processing

The holographic film used for recording was an Agfa–Gevaert, Holotest 10E75 emulsion, 70 mm wide with sprocket holes (Kodak type II perforations) in 600-ft rolls, coated on a polyester base. The laser-induced boiling and stray light limited the peak power density that could be used for the exposure of the film. Therefore, a special processing technique was required which increased the sensitivity of the film and, in particular, reduced the influence of the high intensity re-

ciprocity failure *. The developer utilized the superadditive effect of phenidone (1-phenyl-3-pyrazolidone) combined with hydroquinone. A standard Kodak D-19b developer was used to which 1.5 g/l phenidone was added [35].

Amplitude transmission holograms were produced, which required only development and fixing. The holographic film produced during the run was developed in a modified Kodak Versamat processing machine by a commercial holographic company. Latent image fading slows down when the emulsion is kept cold and therefore exposed rolls were kept in a refrigerator until they were processed. The variation in obtained optical density at the processing stage due to variations in exposure and fading [36], could be compensated for to a certain degree by adjusting the development time or temperature.

A H & D density–exposure plot for holograms is shown in fig. 18a, together with the amplitude transmittance curve in fig. 18b, for our exposure and development of the Agfa–Gevaert 10E75 emulsion.

4.8. Quality of holograms

A virtual image reconstruction machine was built at Fermilab [15] to replay holograms during the run for quality control purposes and for data analysis purposes after the run.

The hologram quality was monitored during the physics run by immediately developing the last 20 frames of each roll removed from the camera. The optical density of these holograms was measured at five spots per frame using a standard densitometer. A delicate balance had to be maintained between sending enough laser light into the Chamber to give a useful hologram density and not sending too much, which would generate excessive microboiling resulting in additional noise light reaching the film and reducing hologram quality. Typical base fog density of the film was 0.2 and we obtained the best results when the hologram had a total density of 0.6; total densities of 1.0 or more resulted in useless holograms. A subset of holograms used for monitoring was looked at using a diverging helium–neon laser beam (virtual image system) and the overall quality of each of them was recorded. A good indicator of the hologram quality was the image visibility and sharpness of various beam reflections (fish-eye reflections, dispersing-lens mount reflection), as well as of the tracks visible in the hologram.

---

* According to the reciprocity law the same photographic density is obtained as long as the product of light intensity with time of illumination is constant. This law fails when either the exposure time is extremely short or the intensity extremely high.

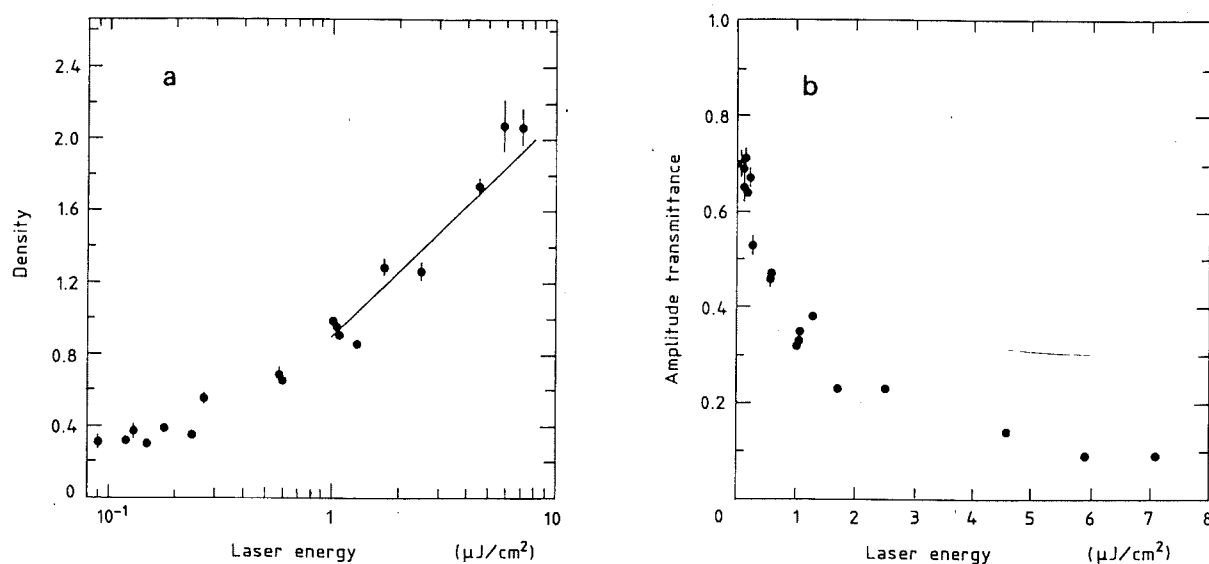Fig. 18. (a) Hurter and Driffield curve, measured for $\lambda = 694.3$ nm, pulse duration $\tau = 2.5$ μs and our development conditions of the Agfa–Gevaert 10E75 emulsion; (b) same results in an amplitude transmittance vs laser energy plot.

This information was then correlated with the data provided by the laser beam monitoring system [23]. This would indicate whenever a change in the operating conditions of the Bubble Chamber or the laser was necessary.

As mentioned in the Introduction to this paper, out of ~ 218 000 holograms about 110 000 (based on the preliminary checks described above) have sufficient track quality to be useful for a physics analysis. Only after all the holograms, together with the conventional photographs and the timing information from the electronic counters have been studied in detail, it will be possible to give a definite breakdown of the variety of reasons contributing to the efficiency factor of ~ 50%. However, we can already name some adverse effects, leading to bad holograms:

(a) instabilities of the illumination system;

(b) thermodynamics of Bubble Chamber operation and purity of its liquid; and

(c) timing problems (event trigger).

All important information about the operation of the laser for each firing is stored on EMI tapes [27] and will be compared on a pulse by pulse basis with the corresponding hologram.

Some loss of good holograms was due to delays involved changing the operating temperature of the almost 20 t of cryogenic liquid, and to unstable startup conditions of the Chamber after extended scheduled standby periods.

4.9. Track properties in holograms

During warm tests in the open Chamber objects were photographed holographically inside the vessel at various positions. We chose glass beads of 100-μm diameter glued on to 20-μm wires, as well as a USAF resolution test target. Satisfactory results were obtained irrespective of the pulse duration, to be expected since their are no vibrations from the expansion system. The one-track (one-line) resolution was 125 μm, or in the usual optical definition, two tracks (two lines) whose centers were separated by 250 μm could be distinguished according to the Rayleigh criterion.

Preliminary measurements of bubble diameters and track resolution [37,38] were made on the Fermilab Virtual Image Replay Machine [15]. The system magnification was measured by placing the USAF target in the virtual image volume and photographing it. The photograph was then digitized giving the system magnification in respect to the pixel elements of the linear CCD array. The linear array used has 1024 pixel elements with 25-μm center to center spacing and was used in conjunction with the Fermilab MOMM film measuring machines.

The spatial coordinates of events in the Bubble Chamber were measured in the conventional stereo views, and this provides the holographic magnification for an event. Photographs of events in the hologram were made with various illumination intensities and exposure times, and were analyzed with the linear array. The bubble diameter is defined as the full width at half maximum of the image above background noise, usually measured on the film with a microdensitometer or a similar device. The average speckle size agrees well with the theoretical value of ≤ 100 μm, calculated for coherent light for the diffraction limit of a point source [39], not taking into account the fish-eye lenses. The calculated diffraction limited resolution at the center of the
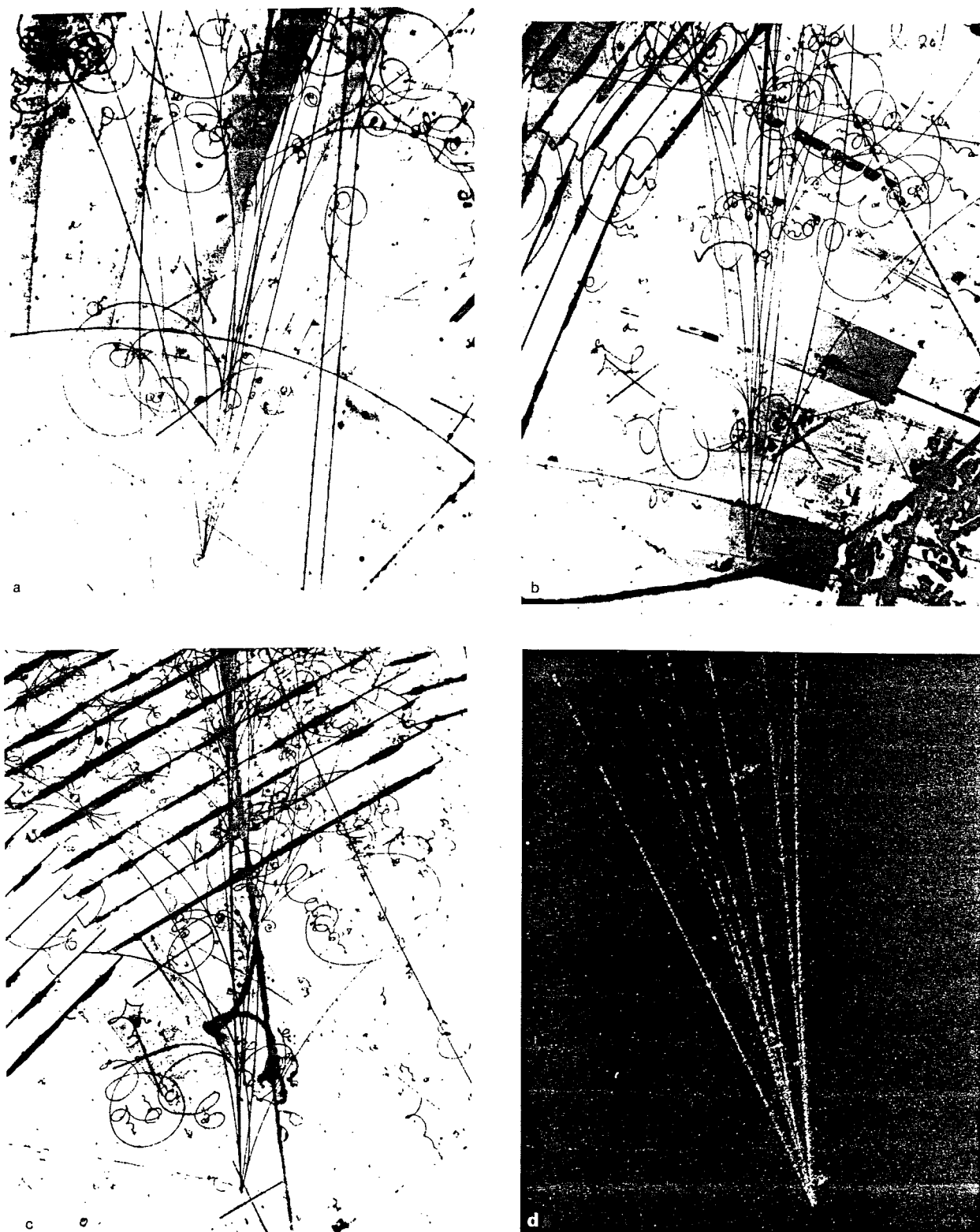
Fig. 19. Comparison of a conventionally and holographically recorded neutrino interaction: (a), (b), (c) photos taken with three conventional cameras; (d) hologram; and (e) interpretation of the event (schematic), 1, 3, 4, 5 are charged particles, and 2 is a particle decaying into C1, C2, C3.
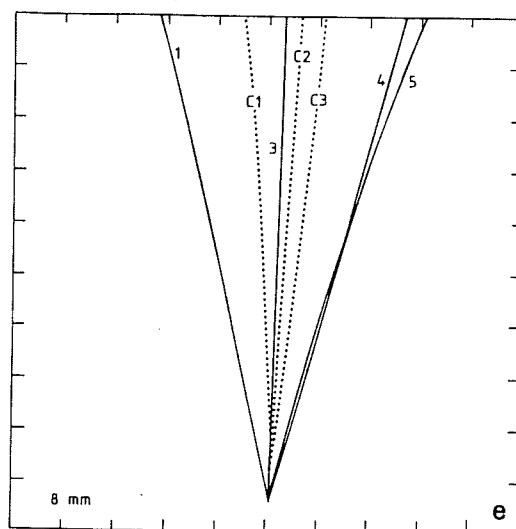
Fig. 19 (continued).

Chamber, i.e. at a distance 2 m away from the film, for a circular hologram area 50 mm in diameter is ~ 43 μm (without fish-eye lenses). Bubbles as small as ~ 100 μm were recorded and replayed with good contrast [38], corresponding to a resolution of ~ 113 μm (according to the Rayleigh criterion), in very reasonable agreement with the bubble size expected from the theory of bubble growth and measured time delay when the hologram was taken. However, the average bubble size during the run was ~ 120 μm, corresponding to a resolution of ~ 135 μm. The track separation was found to have about the same value. The result is in agreement with roughly measured bubble sizes on two real image replay facilities [12,13].

The comparison of an interesting neutrino interaction, photographed with three conventional cameras (figs. 19a–19c), with its recorded hologram (fig. 19d) shows the significant difference in resolution. Whereas in all conventional views nothing spectacular near the neutrino interaction is visible, we see in the hologram a secondary vertex close (0.7 cm) to the primary. This secondary vertex is consistent with the decay of a D^+ charmed meson into three charged mesons plus neutral mesons (schematic drawing fig. 19e). The neutral mesons decay; the resulting photons then convert into electron–positron pairs which are measured in the conventional Bubble Chamber photographs.

4.10. Beam branching ratio

An important quantity in the design of the dispersing lens, and ultimately for the quality of the holograms and the size of the visible volume, is the Minimum Beam Branching Ratio, which was assumed to be 0.33×10^{-7} [40] (section 2.1).

A sample of 1650 holograms has been scanned at the Fermilab replay machine for neutrino interactions. The following cuts have been made on the event sample. It was required that the events are in the fiducial volume of the Bubble Chamber and satisfy the cut $\Theta_i \leq 30°$. The position of the event vertices was measured from the conventional film, which allowed calculation of the geometrical quantities. The bubble growth time of the event was determined from the difference in Pockels cell trigger time and event trigger time, which was determined using the hit patterns in two electronic detectors installed outside the active volume of the Bubble Chamber (IPF, EMI). If there was some ambiguity in assigning the event with the hit pattern, it was removed from the sample. This is mainly the case for events with low track multiplicity, events with none of the particles leaving the liquid volume, or events located in a frame where another event was found. After these cuts the sample contained 51 events.

An estimate of the bubble diameter was obtained using the formula $D = 2A\sqrt{t}$ and assuming $A = 0.2$ cm/s$^{1/2}$ (120-μm bubble diameter after a growth time of 1 ms). The theoretical estimates for $F(\Theta_i)$, $G(\alpha)$ and I_r were used. The input profile of the laser beam was assumed to be flat over the diameter of the lens.

The BBR distribution is shown in fig. 20. One event has a BBR which is less than 0.33×10^{-7}, the maximum BBR is 0.2×10^{-5}. In fig. 21 the holographic z coordinate is plotted vs the illumination angle and contains seen and unseen events. Most of the events, which were predicted from the analysis of the conventional film, but were not found on holograms, were on the borderline of the illumination cone. This could indicate that a higher laser intensity in this region would have resulted in the visibility of the missing events. The volume
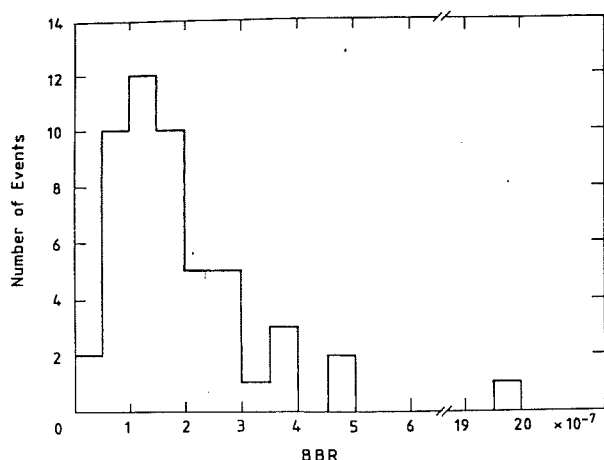
Fig. 20. Beam Branching Ratios of 51 event vertices found in 1650 holograms.

visible in the holograms was determined from this preliminary study to be ~ 1.5 m³.

The fact that an event with BBR $= 0.33 \times 10^{-7}$ has been found indicates, that the assumption of the minimum visible BBR for the design of the dispersing lens was correct.

5. Conclusions

Holographic recording of neutrino interactions in a large Bubble Chamber was successfully done for the first time on a production scale. At least 1.5 m³ of the Fermilab 15-Foot Bubble Chamber's volume was photographed with a resolution which approached 100 μm,

being better than four times the resolution of its standard optics in the middle plane of the Chamber. This allowed the study of close-in interactions and decays in a substantial part of the Chamber with greatly improved precision, leaving enough track lengths outside this volume for measurement of the momentum and identification of particles. The evaluation of these photographs and holograms is in progress.

Several new techniques were developed and successfully implemented. They comprise the design of
a) an innovative pulse-stretching circuitry with adjustable pulse length for a powerful holographic laser,
b) an optical relay system to transport the beam with undiminished quality over a large distance, and
c) an on-line monitoring system of the spatial and temporal features of the laser beam pulse-by-pulse. Furthermore,
d) the holographic film sensitivity was improved by special development techniques,
e) real- and virtual-image replay machines for the holograms were constructed and operated reliably according to design.

The heat absorption of intense laser light light in a cryogenic liquid was studied in some detail and may help to understand better the bubble creation mechanism. It could be shown that bubble tracks could be holographed with good contrast with a Minimum Beam Branching Ratio as small as 0.33×10^{-7}.

Many of these developments may find further interesting applications in the design of a holographic bubble chamber, to be used as the vertex detector within a neutrino hybrid spectrometer, for a 3-TeV accelerator under construction (UNK), and also outside the field of elementary particle physics.
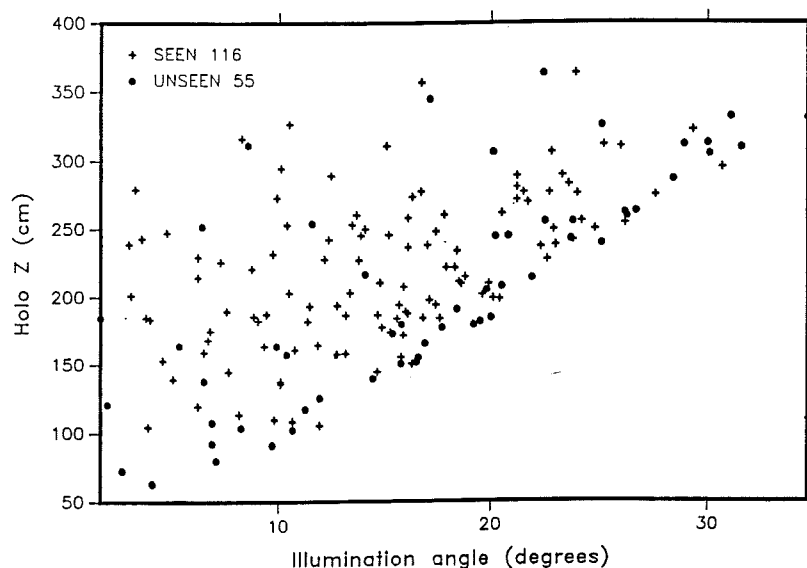

Fig. 21. Scatter plot of seen and unseen events (one holographic roll): holographic z axis versus illumination angle.

References

[1] M. Dykes et al., Nucl. Instr. and Meth. 179 (1981) 487.
[2] A. Hervé et al., Nucl. Instr. and Meth. 202 (1982) 417.
[3] C. Baltay, M. Bregman, M. Hibbs, A. Schaffer, G. Harigel, F. Eisler, R. Cence, E.B. Brucker and T. Hart, Holography in Large Bubble Chambers, Fermilab 15' B.C. and CERN BEBC, talk at BEBC Users Meeting, CERN (1982).
[4] T. Kitagaki et al., Nucl. Instr. and Meth. A281 (1989) 81.
[5] R. Cence, Holography Development, University of Hawaii, int. rep. JR-85-82 (1982).
[6] H. Bjelkhagen et al., Nucl. Instr. and Meth. 227 (1984) 437.
[7] G. Harigel et al., Holographic Recording of Cosmic Ray Tracks in BEBC, in: Photonics Applied to Nuclear Physics, 2, Nucleophot, Strasbourg (1984) p. 69.
[8] H. Akbari and H.I. Bjelkhagen, SPIE 615 (1986) 7.
[9] G.G. Harigel (E-632 Collaboration), Nucl. Instr. and Meth. A257 (1987) 614.
[10] G.G. Harigel (E-632 Collaboration), Nucl. Instr. and Meth. A279 (1989) 249.
[11] H. Akbari, High Resolution Imaging of Particle Interactions in a Large Bubble Chamber using Holographic Techniques, thesis, Tufts University (1987) unpublished.
[12] M.W. Peters and R.J. Cence, Design, Construction and Testing of a Holographic Measuring Machine, in: Photonics Applied to Nuclear Physics, 2, Nucleophot, Strasbourg (1984), p. 95.
[13] M. Aderholz et al., Nucl. Instr. and Meth. A284 (1989) 311.
[14] E.B. Brucker, D. DeProspo, J. Doroshenko, P. Jacques, M. Kalelkar, E.L. Koller, M. Lauko, R. Plano and P. Stamer, The Rutgers Holographic Analysis Machine (HAM), Rutgers University. int. rep. (1988) unpublished.
[15] R. Naon et al., Nucl. Instr. and Meth. A283 (1989) 24.

[16] H. Bjelkhagen et al., Nucl. Instr. and Meth. 220 (1984) 300.
[17] R.J. Withrington, Appl. Opt. 7(1) (1968) 175.
[18] G. Horlitz, S. Wolff and G. Harigel, On the Thermodynamics of Bubble Chamber Expansions, DESY 68/43 (1968).
[19] G. Harigel, G. Horlitz and S. Wolff, On the Movement of Bubbles in a Medium-Sized Bubble Chamber, DESY 72/16 (1972).
[20] G. Harigel et al., Appl. Opt. 25 (1986) 4102.
[21] J.K. Hawkins and W.A. Williams, Proc. Int. Conf. on Lasers-86, STS Press McLean, VA (1987) 553.
[22] L. Verluyten et al., Nucl. Instr. and Meth. A292 (1990) 313.
[23] L. Verluyten et al., Nucl. Instr. and Meth. A292 (1990) 571.
[24] M. Hibbs, Laser Dispersing Lenses for Holography in Large Bubble Chambers, int. rep., Columbia University (1984) unpublished.
[25] 15-Foot Bubble Chamber Safety Report, National Accelerator Laboratory, Batavia, IL (1972).
[26] H. Foeth, Nucl. Instr. and Meth. 176 (1980) 203.
[27] V. Jain et al., Phys. Rev. D41 (1990) 2057.
[28] P.P. Allport and E. DeWolf, Fast Event Trigger for Holography or High Resolution Camera HRC, int. rep. E632 collaboration (1985).
[29] J. Badier et al., Chambre à Hydrogène à Haut Taux de Repetition, Rapport CEA-R 3144 (1967), Centre d'Etudes Nucléaires de Saclay, France.
[30] F.H. Poesposoetjipto and E. Hugentobler, Helv. Phys. Acta 43 (1970) 203.
[31] G. Horlitz, S. Wolff and G. Harigel, Nucl. Instr. and Meth. 117 (1974) 115.
[32] S. Wolff, Blasenbildung und Blasenwachstum in einer mit Wasserstoff und Deuterium gefüllten Blasenkammer, dissertation, Hamburg (1969) unpublished.
[33] G. Horlitz, S. Wolff and G. Harigel, Nucl. Instr. and Meth. 115 (1974) 365.
[34] G. Harigel et al., Nucl. Instr. and Meth. 188 (1981) 517.
[35] H. Bjelkhagen, Holographic Recording Materials and the Possibility to Increase their Sensitivity, CERN/EF 84-7 (1984) unpublished.
[36] Holographic Group, Latent-Image Fading, Fermilab, int. note (1987) unpublished.
[37] R. Naon, Search for Short-Lived Decays Produced by Tevatron Neutrino Beam using Holographic Optics, int. rep. IIT, Chicago, USA (April 1988) unpublished.
[38] R. Naon, Investigation of Bubble Diameters and Holographic Resolution, int. rep. IIT (1987) unpublished.
[39] M. Young, B. Faulkner and J. Cole, J. Opt. Soc. Am. 60 (1970) 137.
[40] L. Verluyten, Use of Holographic Optics to Obtain High Resolution over a Large Volume to Search for Short Lived Particles, IIHE-88.01 rep., Brussels, Belgium, (1988) unpublished.